applied sciences

MDPI

Article

The Study of Triangular Flow Regulators

Marek Ochowiak [1], Magdalena Olszewska [1,2], Daniel Janecki [3], Sylwia Włodarczak [1], Andżelika Krupińska [1] and Magdalena Matuszak [1,*]

[1] Faculty of Chemical Technology, Poznan University of Technology, 60-965 Poznan, Poland; marek.ochowiak@put.poznan.pl (M.O.); magdalena.olszewska@pbs.edu.pl (M.O.); sylwia.wlodarczak@put.poznan.pl (S.W.); andzelika.krupinska@put.poznan.pl (A.K.)
[2] Faculty of Chemical Technology and Engineering, Bydgoszcz University of Science and Technology, 85-796 Bydgoszcz, Poland
[3] Institute of Environmental Engineering and Biotechnology, University of Opole, 45-035 Opole, Poland; zecjan@uni.opole.pl
* Correspondence: magdalena.matuszak@put.poznan.pl

Abstract

The paper presents the results of tests of flow regulators with a triangular prismatic cross-section chamber. The aim of the paper was to experimentally and numerically (CFD) assess the water flow for different design variants of the regulators. Three variants of flow regulators with a triangular prismatic cross-section chamber were analysed: without a barrier (FRWB), with a short barrier (FRSB), and with a long barrier (FRLB). Simultaneously, numerical simulations were carried out using the SST k-ω turbulence model (CFD). The obtained flow characteristics $Q = f(H)$ showed the clear effect of the presence and length of the barrier on the efficiency of flow restriction. The regulators with a long barrier (FRLB) provided the highest flow damping and the highest stability of the system's operation, which was confirmed by the experimental tests and CFD analyses. The regulators without a barrier (FRWB) were characterized by the highest liquid flow rate and the lowest damping efficiency. The use of a long barrier allowed for an increased control efficiency and improved predictability of the device's operation. The triangular cross-section of the chamber favours the formation of a stable vortex flow and increases the efficiency of the regulator's operation.

Keywords: flow regulators; discharge coefficients; CFD analysis

check for updates

Academic Editors: Reza Hassanian and Morris Riedel

Received: 6 October 2025
Revised: 6 November 2025
Accepted: 19 November 2025
Published: 20 November 2025

Citation: Ochowiak, M.; Olszewska, M.; Janecki, D.; Włodarczak, S.; Krupińska, A.; Matuszak, M. The Study of Triangular Flow Regulators. *Appl. Sci.* **2025**, *15*, 12325. https://doi.org/10.3390/app152212325

Copyright: © 2025 by the authors. Licensee MDPI, Basel, Switzerland. This article is an open access article distributed under the terms and conditions of the Creative Commons Attribution (CC BY) license (https://creativecommons.org/licenses/by/4.0/).

1. Introduction

Flow regulators are a key element of hydraulic infrastructure. They enable the control of the liquid flow rate and the stabilization of flow conditions in sewage, retention and industrial systems. Their use reduces the probability of the hydraulic overload of a system [1]. Flow can be regulated using various techniques [2]. Passive hydrodynamic flow regulators are a durable and cost-effective alternative to the traditional devices that are commonly used in urban infrastructure [3]. A special group consists of vortex regulators, the operation of which is based on generating an air core in a specially shaped chamber that limits the flow. Forcing the flow through a helical chamber results in sudden expansions and contractions, which in turn cause a high level of turbulence. These turbulences limit the flow rate much more than a cylindrical opening [1]. These devices are distinguished by a simple design (without moving elements), and also a high reliability and resistance to clogging [4]. The first mentions of the application of this type of device in the context of the management of water resources can be found in the literature from the 1980s [5,6]. Despite the growing use of vortex regulators, especially in storm sewers and retention systems,

specialist literature contains little data on the effect of design parameters on the hydraulic characteristics of these devices. Previous studies have focused mainly on vortex diodes that operate bidirectionally and which have been widely studied both experimentally and numerically [7–9]. Although vortex regulators have a relatively simple construction and the nature of the flow in them is unidirectional, the research results related to their operation are still poorly documented in scientific publications. This is due to their unique hydraulic characteristics [4]. Studies by Parsian and Butler [10] showed that in order to obtain comparable control effects, a vortex regulator can have an outlet opening with a diameter 3 to 4 times larger than the diameter of a classic orifice that provides the same flow characteristics. Such a configuration significantly reduces the risk of the device clogging, which is one of the main advantages of the vortex construction when compared to conventional orifice-based solutions. The increased cross-section of the outlet opening makes the device better at transporting pollutants in water, such as mineral and organic suspensions, which in turn makes them particularly useful in storm and retention sewage systems. Siuta and Mączałowski [11] demonstrated that vortex regulators operating at Reynolds numbers exceeding 10^4 can exhibit two distinct, stable flow states—either with or without a developed vortex—under the same liquid head conditions. This phenomenon, known as bistability, means that two different flow regimes can occur at the same head height, depending on whether the liquid level is increasing or decreasing. As a result, there is a hysteresis effect in the $Q = f(H)$ characteristic, which in turn can lead to difficulties in unambiguously determining the discharge coefficient based on the current liquid level. The practical effect of this phenomenon is the possibility of passively limiting the discharge at higher hydraulic loads without the need for mechanical control, which can be beneficial when considering sewage and retention issues. As demonstrated by Kotowski and Wójtowicz [12], in the case of appropriately high Reynolds numbers ($Re > 10^4$), the discharge coefficient has a nearly constant value, which simplifies the hydraulic description of the regulator. However, the efficiency of flow damping significantly depends on the geometric invariants, such as the ratio of the chamber diameter to the regulator's inlet or the vortex radius. The authors emphasize that these relations can be used for the preliminary design of regulators with specific operating parameters. The use of vortex flow regulators can also be found in aeration systems [13]. The authors of the article demonstrated the complexity of the flow of liquid through a cylindrical flow regulator and the influence of design parameters on the efficiency of the conducted process.

In recent years, computational fluid dynamics (CFD) has become an important tool that supports the design and analysis of vortex regulators. Comparing simulation results with experimental ones allows for the optimization of many processes used in industry, for example: in the hydrodynamics of sand-laden wastewater within a spiral separator [14], in hydrodynamic separators with swirling flow which are used to control the total suspended solid concentration in stormwater before being discharged to natural water bodies [15], and in optimization structural parameters by analyzing the effects of Hydrodynamic vortex separators design elements [16]. Weipeng et al. [17] presented the study utilized Computational Fluid Dynamics (CFD) simulation methods to investigate the mechanisms by which different flow states (gravity flow and pressure flow) and pipeline bending angles influence the turbulent dynamics and energy transfer patterns of stormwater manholes. Thanks to the ability to visualize complex hydrodynamic phenomena, such as air core formation, local turbulence zones or pressure losses, CFD simulations enable a preliminary assessment of flow damping efficiency without the need to build physical models. Siuta and Mączałowski [11] used the RANS model with k-ε turbulence to analyse the flow through vortex regulators. The authors demonstrated the consistency of numerical analysis with experimental results and stated that there is a possibility of identifying parameters

that influence the hysteresis effect. Kotowski and Wójtowicz [12] also emphasized the usefulness of numerical modeling for assessing the influence of the controller's geometry on the $Q = f(H)$ characteristics [11,12].

Vortex regulators are currently offered by many manufacturers of devices for water and sewage engineering, which confirms their usefulness in engineering practice. Examples include Hydro-Brake® regulators from Armtec [18]; Tornado, Typhoon and Hurricane devices from Wavin [19]; as well as models offered by Oksydan [20] or Andel [21]. A common feature of these regulators is the lack of moving elements, automatic operation based on the generation of an air core, and high resistance to clogging. These designs are most often based on cylindrical or conical chamber geometry [22–24]. They can be applied in storm sewers, retention tanks, and the separators of petroleum derivatives. Despite the wide use of these solutions, technical literature does not provide sufficient experimental data on the effect of less conventional chamber geometries (such as a triangular prismatic cross-section) and the presence and length of flow-directing elements on flow characteristics and control efficiency. The aim of this paper is to fill this research gap by analysing the influence of both the chamber shape and the design variants of the barriers on the hydraulic parameters of vortex regulators. The authors have conducted and continue to conduct systematic studies on various constructions of flow regulators, including cylindrical, conical [23,25–27], triangular [28,29], and box-type geometries, and cylindrical with a square inlet [30–35]. The choice of a triangular prismatic chamber was motivated by the expected improvement in flow stability and vortex formation. In comparison with cylindrical or conical geometries, the triangular cross-section promotes the development of three distinct circulation zones along the walls, which favour the stabilization of the swirl core and reduce flow asymmetry. Additionally, this geometry is simpler to manufacture using additive methods and allows for easier modular variation in the barrier length.

2. Materials and Methods

2.1. Experimental Procedure

The tests were carried out in laboratory conditions on a measuring stand that enables the gravity flow of liquid through the tested regulators on a pilot scale. The main element of the system was a vertical cylindrical tank with a diameter of 0.2 m and a total height of 2.0 m. It was made of transparent plastic (PMMA), which enabled the ongoing observation of the liquid level and hydrodynamic phenomena. Water at an ambient temperature (approx. 20 °C) was supplied from the water supply network using a flexible pressure pipe with a ball valve at the end. The water supply was manually regulated, which allowed for the precise setting of the desired liquid damming level. The upper part of the tank was open. This enabled venting and prevented the formation of negative water pressure. Inside the tank there was a millimeter scale for reading the height of the water surface. The tested regulators were mounted in the side wall of the tank (at a height of approx. 0.1 m from the base) through a prepared hole with a diameter adapted to the outlet nozzle. The actual method of installing the regulator in the wall of the measuring column is presented in Figure 1. The liquid flow from the regulator was directed to an open measuring vessel (receiving tank) with a capacity of 30 L, which was placed below the stand. The volume of the flowing liquid was measured using the volume-time method—until 10 L of water were collected, the flow time was measured using a stopwatch. The procedure was repeated three times for each level of damming. The measuring system was placed on a stable horizontal base in order to avoid the influence of the inclination on the flow conditions. The main sources of measurement uncertainty were related to the reading of the water column height (±1 mm) and the manual time measurement (±0.1 s). The relative uncertainty of the volumetric flow rate determination was estimated to be below 5% for all test points, based

on repeated measurements. These uncertainties were propagated through the calculation of the discharge coefficient μ to assess the experimental error range.

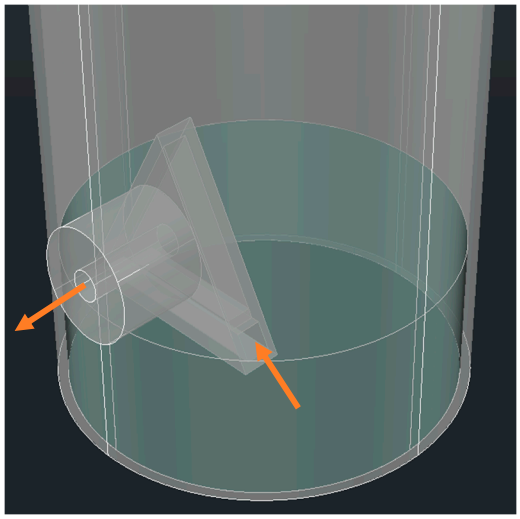

Figure 1. Method of mounting the regulator in the measuring column.

The research involved the use of a set of vortex regulators, which were made of PLA using the 3D printing method in FFF technology. The chamber of each regulator had the shape of a prism with an equilateral triangular base, which was a significant difference when compared to the classically used cylindrical or conical chambers. All the models had similar external dimensions, but variable internal parameters, which allowed for a comparison of their behaviour. The tested regulators were divided into three basic construction types that differed in terms of the presence and length of the flow-directing barrier: FRWB (Flow Regulator Without Barrier)—a model without a barrier, which allows for free flow in the entire volume of the chamber; FRSB (Flow Regulator with Short Barrier)—a model with a barrier with a length equal to the diameter of the inlet, which was mounted at the wall adjacent to the inlet; and FRLB (Flow Regulator with Long Barrier)—a model with a barrier that had a length selected so that between its end and the inner wall of the chamber opposite the inlet there was a gap with a width equal to the diameter of the inlet (directing the flow in a way similar to the classic vortex concepts). In all the variants, identical mounting points were used for the inlet and outlet. The inlet was located in one of the side walls and had a tangential character, which initiated the swirling motion of the liquid. The outlet was placed centrally in the base of the regulator's chamber. Moreover, four geometric variants were used. They differed with regards to the cross-sectional area of the inlet and outlet openings, which in turn allowed for the assessment of the effect of the inlet to outlet diameter ratio on the value of the discharge coefficient μ and the efficiency of flow attenuation. All the models were designed in Autodesk AutoCAD 2024. The models consisted of interchangeable structural elements, which, when assembled, created a tight and stable whole. Such an arrangement allowed for a quick modification of the regulator's geometry without the need to print monolithic elements. The regulators were used many times in the tests, and their technical condition was checked before each measurement series.

Figure 2 shows three design variants of the regulators. Differences in the shape of the internal partition are visible—the model without a barrier allows for free circulation of the liquid in the entire space of the chamber, the variant with a short barrier initiates swirl at the side wall and partially directs the stream, while the long barrier effectively limits the flow space by forcing the liquid to swirl around the chamber.

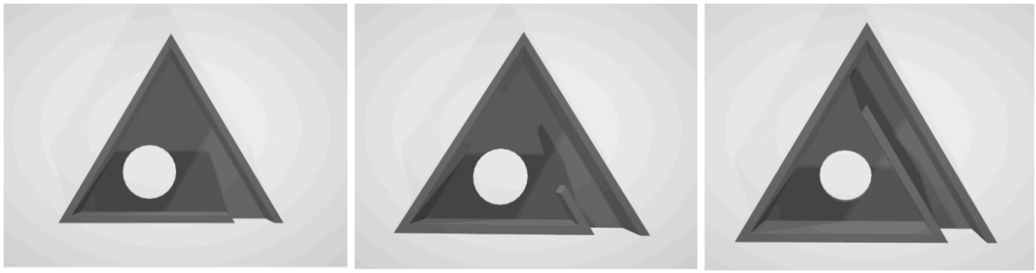

(**a**) (**b**) (**c**)

Figure 2. Different variants of triangular vortex regulators: (**a**) without a barrier; (**b**) with a short barrier; (**c**) with a long barrier.

Figure 3 shows photos of real models of the FRLB flow regulator made using FFF technology: (a) isometric and (b) frontal. The design was developed with the intention of forcing the swirl flow by using the appropriate arrangement of holes and an internal guiding barrier. The isometric view allows the arrangement of the inlet nozzle in relation to the side wall of the chamber to be observed, and its tangential nature to be indicated. Such a position favours the initiation of swirl motion and the generation of the liquid torque already in the initial phase of the inflow. In this view, the internal barrier is also visible. It is oriented parallel to one of the walls, and its task is to direct the stream and limit the effective cross-section of the flow. In turn, the frontal view reveals the central location of the outlet's opening in the base of the chamber, and the spatial arrangement of the barrier in relation to the axis of the regulator. In this case, the barrier plays the role of an element that separates the circulation of the swirling liquid from the outflow axis, which in turn favours the formation of an air core. This type of stabilized swirl flow system, with a clear effect of centrifugal forces and reduced pressure in the chamber axis, enables the effective limitation of the kinetic energy of the stream and the effective control of the outflow rate. The presented views allow for a more complete interpretation of the geometry of the structure, which, in combination with the measurement results and numerical analysis, provides a basis for assessing the efficiency of the regulators.

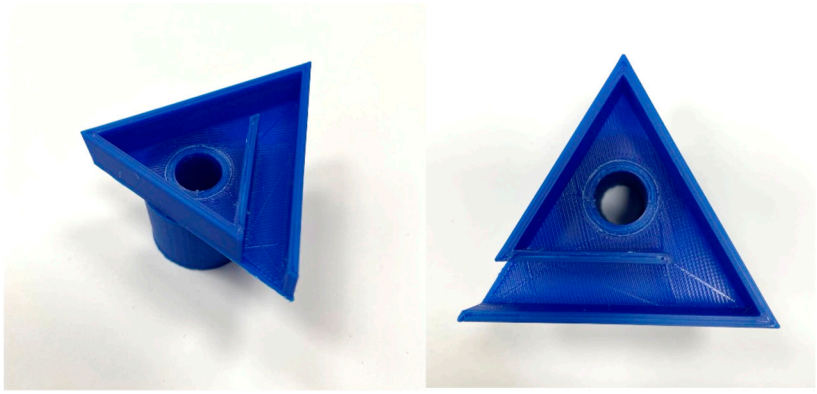

(**a**) (**b**)

Figure 3. View of the flow regulator: (**a**) isometric—arrangement of the inlet's opening and barrier; (**b**) central.

Detailed geometric documentation of the tested regulators is presented in Figure 4 and Tables 1 and 2. In order to enable the comparison of different design configurations, a set of models with similar external dimensions, but variable parameters that are important from the point of view of flow, was prepared. Four dimensional series, which differed in terms of the diameters of the inlet and outlet openings and the height of the chamber, and three design types, differing in terms of the length of the internal barrier, were taken into

account. These variants allowed for the analysis of the influence of the geometry on the hydraulic parameters of the vortex flow.

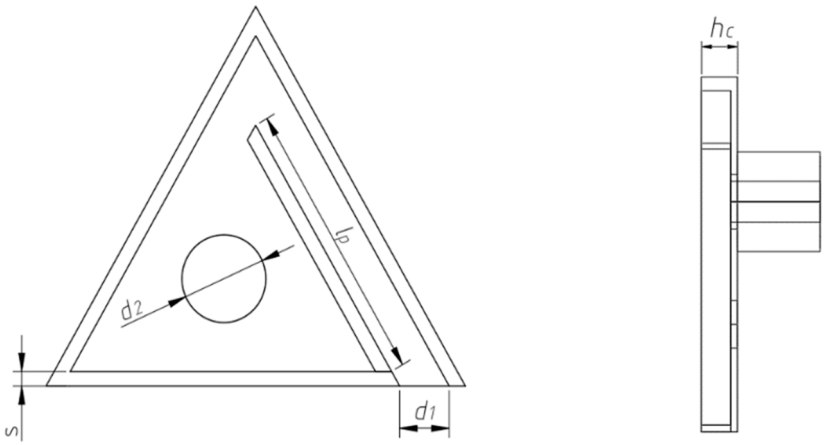

(**a**) (**b**)

Figure 4. Orthogonal projections: (**a**) front; (**b**) side; designations: d_1—equivalent inlet diameter; d_2—outlet diameter; l_p—partition length; s—wall thickness; h_c—height of the regulator's chamber.

Table 1. Dimensions of individual types of triangular flow regulators.

Series	d_1 (m)	d_2 (m)	h_c (m)
1	0.00725	0.00760	0.00985
2	0.00930	0.00945	0.01135
3	0.01070	0.01160	0.01335
4	0.01240	0.01330	0.01535

Table 2. Dimensions of barriers for individual controller models and individual measurement series.

Series	FRLB				FRSB				FRWB
Series	1	2	3	4	1	2	3	4	-
Barrier length l_p (m)	0.0393	0.0356	0.0324	0.0285	0.00735	0.00920	0.01090	0.01270	-

A thorough understanding of the operation of vortex regulators requires the determination of the basic relationships that describe the flow of liquid through the device's chamber. The main calculations were based on classical hydrodynamic relationships and experimental data obtained during the laboratory measurements.

The basic operating parameter was the liquid volume flow, which was determined according to the following relationship:

$$Q = \frac{V}{t} \tag{1}$$

where Q—volumetric flow rate (m^3/s), V—volume of the collected liquid (m^3), t—flow time of the collected liquid (s).

To classify the type of flow in the system, the Reynolds number was used, which was calculated according to the following equation:

$$Re = \frac{2\rho Q}{\pi \eta r_1} \tag{2}$$

where ρ—density of the liquid (kg/m^3), r_1—equivalent inlet opening radius (m), η—dynamic viscosity of liquids (Pa·s).

The discharge coefficient μ is one of the key parameters for assessing the efficiency of a vortex regulator. It was calculated based on the modified Torricelli formula:

$$\mu = \frac{Q}{A_1\sqrt{2g\Delta H}} \quad (3)$$

where A_1—outlet opening area (m^2), ΔH—height of liquid damming above the outlet axis (m).

The values of the discharge coefficient were determined for each measurement series and then compared as a function of the Reynolds number, which enabled the analysis of the dependence of the hydraulic characteristics on the flow's conditions. Detailed results are presented later in the paper together with the $Q = f(H)$ characteristic graphs and $\mu = f(Re)$.

2.2. Numerical Modeling

2.2.1. Numerical Analysis

The numerical analysis was carried out independently from the experiments, using the same geometric and boundary parameters for validation purposes. The initial and boundary conditions used in the CFD modelling of the flow regulators were based on the experimental data. At the inlet, a pressure inlet boundary condition was used, in which hydrostatic pressure corresponding to the height of the liquid column in the supply system was assumed. At the outlet, a pressure outlet condition was assumed, which allows for the atmospheric pressure to be defined as the reference pressure.

In order to select the optimal computational grid, a grid independence study was conducted using several grids with different density and element distributions. The tested grids differed in terms of the number of elements. The main evaluation parameter was the flow rate at the regulator's outlet, which is considered to be a sensitive indicator of the quality of the mapping of the grid in the flow system. The analysis compared four unstructured grids with the following number of elements: 35,838, 67,748, 101,030 and 141,919. The results presented in Table 3 indicate that for the grids containing more than 100,000 elements, the further increasing of the number of elements did not lead to a significant improvement in the accuracy of the results—the differences in flow were insignificant and within the numerical tolerance. In turn, for the grids with a smaller number of elements, a deterioration in the accuracy of the flow mapping was observed, despite the shorter computation time. On this basis, the grid with 101,030 elements was adopted for further calculations, and was considered to be optimal in terms of the ratio of the quality of results to the simulation time. The selection of this grid ensured numerical stability and a satisfactory convergence of results, while at the same time maintaining reasonable computational resources.

Table 3. Grid vs. flow rate.

Grid (Number of Elements)	Flow Rate (m^3/s)	μ [-]
35,838	0.000411	0.5453
67,748	0.000378	0.5015
101,030	0.000399	0.5294
141,919	0.000400	0.5307

2.2.2. Governing Equations and Modelling Assumptions

Water was modelled as single-phase, incompressible, isothermal at T = 20 °C with density ρ = 998.2 (kg/m^3) and dynamic viscosity $\eta = 1.003 \times 10^{-3}$ (Pa·s). Simulations used gauge pressure, with operating pressure set to p_{atm} = 101,325 (Pa). Transient free-surface

and entrained-air effects were not included. The present CFD is therefore intended to capture trend-level hydrodynamics under fully flooded conditions.

The steady Reynolds-Averaged Navier–Stokes (RANS) equations were solved:

$$\nabla \cdot u = 0 \tag{4}$$

$$\rho(u \cdot \nabla)u = -\nabla p + \nabla \cdot \left[(\eta + \eta_t)\left(\nabla u + (\nabla u)^T\right)\right] \tag{5}$$

where u is the mean velocity, p the mean pressure, and η_t the eddy viscosity.

Turbulence closure used the SST k-ω model. The transported scalars are turbulent kinetic energy k and specific dissipation rate ω:

$$\rho(u \cdot \nabla)k = \nabla \cdot [(\eta + \sigma_k \eta_t)\nabla k] + P_k - \beta^* \rho k \omega \tag{6}$$

$$\rho(u \cdot \nabla)\omega = \nabla \cdot [(\eta + \sigma_\omega \eta_t)\nabla \omega] + \alpha \frac{\omega}{k} P_k - \beta \rho \omega^2 + (1 - F_1) 2\rho \sigma_{\omega 2} \frac{1}{\omega} (\nabla k \cdot \nabla \omega) \tag{7}$$

with the standard SST coefficients and production limiter [36].

2.2.3. Computational Domain and Boundary Conditions

The simulated geometry reproduced the test regulators (triangular cross-section body and FRWB/FRSB/FRLB inserts, dimensions in Tables 1 and 2). The inlet was prescribed as a pressure inlet representing a hydrostatic head ΔH above the device datum. To enforce the correct vertical pressure variation, the total pressure was applied via a user-defined function (UDF). Turbulence at the inlet used 5% and a turbulent viscosity ratio of 10. The hydraulic diameter at the inlet was set to $D_h = d_1$ for the circular inlet and $4A/P_{wetted}$ for the non-circular case (where A is the inlet flow area and P_{wetted} the wetted perimeter). The outlet was a pressure outlet at atmospheric pressure with backflow turbulence identical to the inlet. All solid walls were no-slip. No symmetry planes were used.

2.2.4. Mesh and Near-Wall Treatment

The domain was discretized with an unstructured poly/trim mesh and prism (inflation) layers on all walls to resolve near-wall gradients. Near-wall resolution was chosen to keep y^+ in the low-to-moderate range compatible with the SST k-ω model. Minimum orthogonal quality exceeded 0.2 and maximum skewness was below 0.85.

A four-level mesh refinement was carried out (G1–G4) to assess the sensitivity of the numerical solution to grid density. The meshes contained 35,838 (G1), 67,748 (G2), 101,030 (G3) and 141,919 (G4) cells, respectively. Since the main objective of the present work is to characterise the hydraulic behaviour of the vortex regulator, the outlet discharge Q and the corresponding discharge coefficient μ were taken as the primary indicators of mesh convergence.

Table 3 summarizes the discharge coefficient μ for all four grids. Taking the 101,030-cell mesh (G3) as the reference, the coarsest mesh (G1) overpredicts μ by 3.01%, the intermediate mesh (G2) underpredicts it by 5.26%, while the finest mesh (G4) differs from G3 by only 0.25%. This demonstrates that the discharge-related quantities stabilise for the two finest grids and that G3 represents a good compromise between accuracy and computational cost.

To document wall resolution, the Fluent variable Wall Yplus was exported over all solid boundaries for the three finest grids (G2–G4) and post-processed into basic statistics (min, median, mean, 90th, 95th, 99th percentile, and maximum). The results are given in Table 4. They show that most of the wall area lies in the enhanced-wall/wall-function regime, while high y^+ values are confined to small regions near sharp edges and in the intense-swirl zone of the regulator.

Table 4. Wall y^+ statistics exported from Fluent for the three finest grids.

Grid ID	Samples	y^+min	y^+median	y^+mean	y^+90	y^+95	y^+99	y^+max
G2 (67,748 cells)	2780	2.74	13.94	25.89	78.92	84.23	90.37	97.98
G3 (101,030 cells)	8850	2.05	22.54	23.29	41.31	44.07	47.87	62.60
G4 (141,919 cells)	4535	1.20	29.11	30.33	54.36	58.94	66.05	81.64

The increase in the upper-percentile y^+ (P90–P99) for G2 and G4 is associated with sharp internal edges and with the strongly swirling core, i.e., with small parts of the total wall area. The SST k–ω model was therefore used together with the enhanced/blended wall treatment available in Fluent, which supports both low-Re ($y^+ \approx 1$–5) and wall-function ranges on the same mesh. Because the present simulations employed a steady, single-phase RANS model with non-uniform local refinements tailored to the triangular-corner vortices, a formal GCI for the vortex-core length was not computed; instead we report the stabilisation of Q and μ between the two finest grids and the full wall-y^+ distributions as a transparent measure of mesh adequacy.

2.2.5. Numerical Schemes and Solver Settings

All simulations were performed with the commercial finite-volume solver ANSYS Fluent 2023 R2. The pressure-based segregated steady solver was used with: pressure–velocity coupling—SIMPLE (pseudotransient under-relaxation enabled for robustness), spatial discretization—second-order for pressure and second-order upwind for momentum, k, and ω, gradient reconstruction—least-squares cell-based. For each imposed ΔH, the solution was initialized from zero flow and iterated until both residual and monitor convergence were achieved.

2.2.6. Limitations

Because the present model neglects the free surface and air-core dynamics and is solved in steady RANS, it cannot capture hysteresis or bistable regimes sometimes observed in vortex regulators. Consequently, CFD comparisons are interpreted quantitatively with caution and primarily for trend validation against the experiments (Sections 3 and 4). A two-phase transient VOF extension is outlined as future work.

3. Results and Discussion

Figure 5 presents the flow characteristics $Q = f(H)$ for the different design variants of the triangular vortex regulators, including the results of the experimental tests and CFD numerical simulations. The relationships show the effect of the barrier's configuration on the flow damping efficiency.

All the $Q = f(H)$ characteristics show the expected increasing course—with an increase in flow rate, the height of the liquid column also increases. However, a clear difference in the dynamics of the flow increase between the individual design variants is visible. The regulators with a long barrier (FRLB) are characterized by the most limited flow sensitivity to the increase in the damming level, which in turn indicates a high efficiency of the flow damping. The regulators with a short barrier (FRSB) have a moderate ability to limit the increase in flow, while the models without a barrier (FRWB) achieve characteristics with an almost linear dependence of flow to the damming level (indicating low control efficiency).

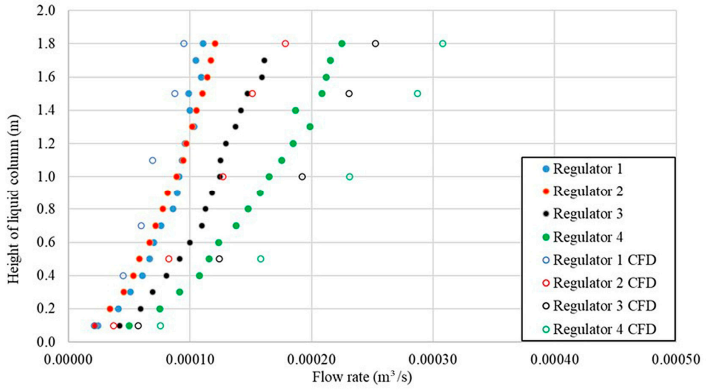

(**a**)

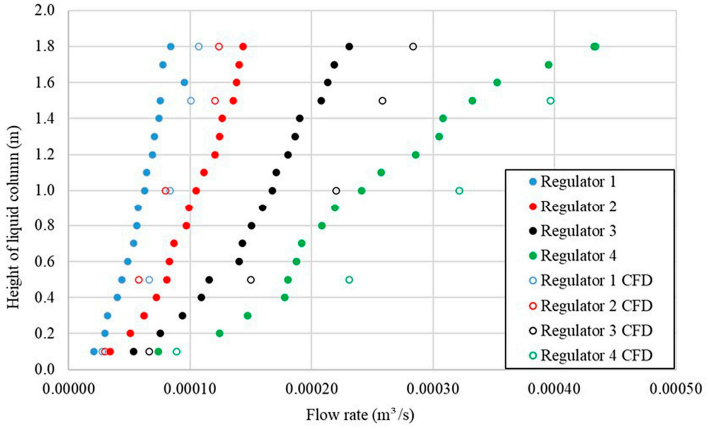

(**b**)

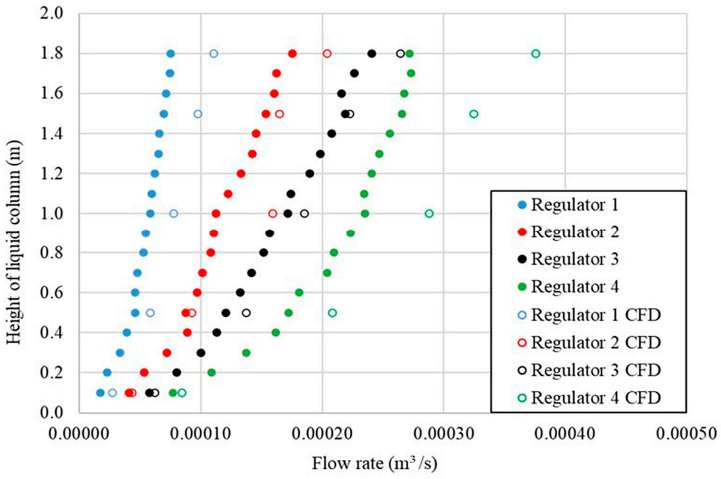

(**c**)

Figure 5. $Q = f(H)$ relationship for regulators: (**a**) with a long barrier (FRLB); (**b**) with a short barrier (FRSB); (**c**) without a barrier (FRWB). The filled symbols represent experimental results, open symbols correspond to CFD data.

In addition, based on the comparison of the measurement series, the influence of the size of the inlet and outlet opening on the flow characteristics was observed. The variants with a larger cross-sectional area of the outlet opening (series 3 and 4) had higher flow rates for the same values of the level of damming when compared to the series with smaller diameters (series 1 and 2). The experimental data shows good agreement with the CFD simulation results. In the case of the regulators with a long barrier (FRLB), the smallest discrepancies between the experimental results and the results obtained from the CFD

analysis were observed for regulator 1, where the average relative error was 24%. For the regulators with a short barrier (FRSB), the highest agreement of the results was obtained for regulator 4. In this case, the average relative error was 16%. In the case of the regulators without a barrier (FRWB), the smallest differences in the values between the experimental data and the results from the numerical analysis were obtained for regulator 3, and the average relative error was 7%. It should be emphasized, however, that the CFD analysis was of an illustrative nature in order to confirm the trend of the hydraulic characteristics obtained from the experimental data. Due to the time-consuming and complicated process of determining the conditions for conducting the numerical analysis, the flow rates were determined for five selected liquid damming levels.

Figure 6 presents the dependencies of $\mu = f(Re)$ for the different measurement series of the triangular vortex regulators, including the results of the experimental tests. The dependencies show the influence of the barrier's configuration and geometrical dimensions on the stability of the regulator's operation. The graphs are supplemented by the average values of the discharge coefficient, which was listed in Table 5.

Table 5. Experimental values of the discharge coefficients for a turbulent flow.

Type	Series	Discharge Coefficient for a Turbulent Flow (-)
FRWB	1	0.314
	2	0.404
	3	0.433
	4	0.424
FRSB	1	0.343
	2	0.357
	3	0.421
	4	0.492
FRLB	1	0.496
	2	0.295
	3	0.285
	4	0.310

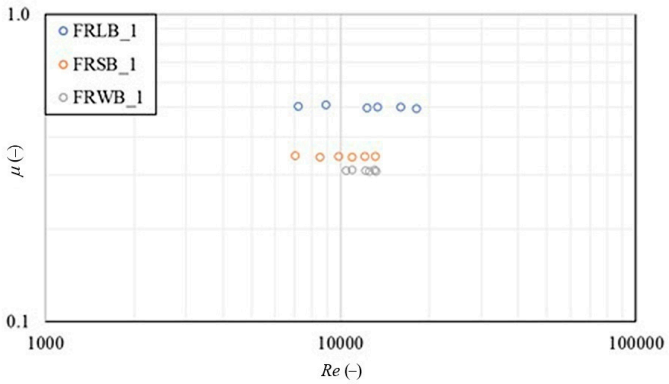

(**a**)

Figure 6. *Cont.*

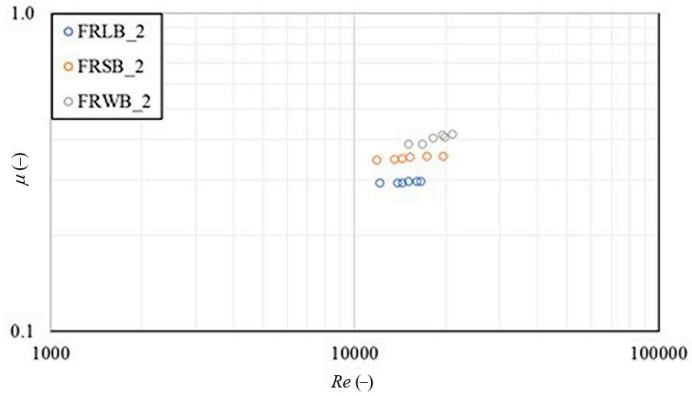

(**b**)

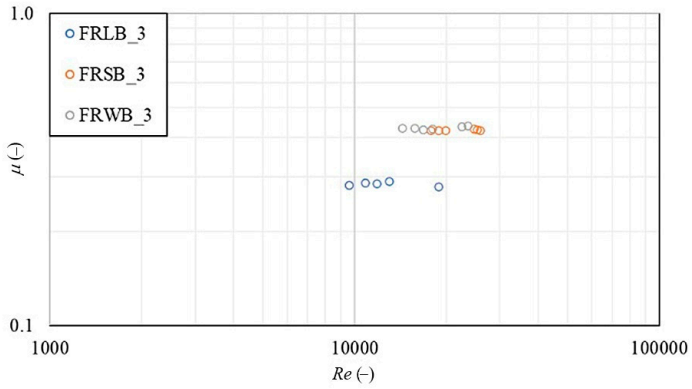

(**c**)

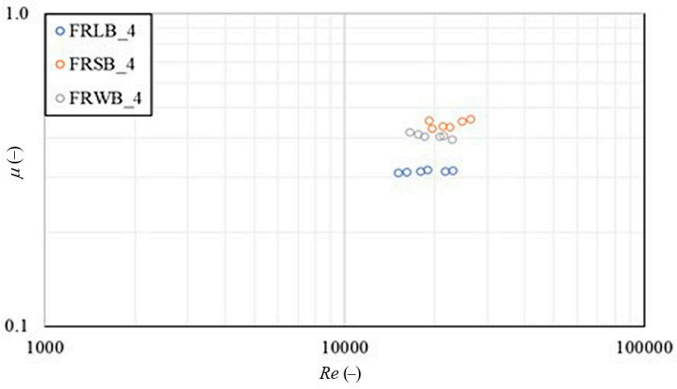

(**d**)

Figure 6. Dependence of the discharge coefficient on the Reynolds number for the flow regulators: (**a**) series 1; (**b**) series 2; (**c**) series 3; (**d**) series 4.

The regulators with a long barrier (FRLB) generally achieved the lowest discharge coefficient values among all the tested design variants. However, the results differed significantly depending on the geometric variant. For series 2 and series 3, the lowest μ values (0.285 and 0.288, respectively) were recorded, and at the same time high stability of the coefficient value as a function of the Reynolds number was maintained. This indicates very effective flow damping and a strong stabilization of the swirl motion. In series 1, the μ value was equal to 0.496, whereas for series 4 it was 0.310 higher than in series 2 and 3. This was associated with a lower share of swirl motion and the occurrence of the stream contraction effect. In the case of the regulators with a short barrier (FRSB), the discharge coefficient values were within the range of 0.343–0.492. The lowest value was recorded in the case of series 2 (0.357), whereas the highest in the case of series 4 (0.492). Analysis

of the $\mu = f(Re)$ dependence showed a slightly larger scatter of values, especially in the case of the lower Reynolds ranges. This indicates a lower efficiency of flow stabilization when compared to the FRLB model. The regulators without a barrier (FRWB) achieved μ coefficient values within the range from 0.314 to 0.433. The lowest value was obtained in the case of series 1 (0.314), whereas in the case of series 3 and 4 the values were clearly higher (0.433 and 0.424). In turn, the $\mu = f(Re)$ characteristics showed the greatest variability, which indicates a lack of flow stabilization.

Figure 7 shows examples of velocity field and velocity vector distributions, which were obtained from the CFD simulations conducted for the regulators with a long barrier (FRLB) and for a liquid damming of 1.5 m. These visualizations allow for the identification of the mechanisms that are responsible for an effective liquid flow limitation. Numerical simulations were carried out using the SST k-ω turbulence model, which in turn allows for the faithful mapping of near-wall flows and vortex structures that are characteristic for the analyzed structures.

The velocity vector distributions for the regulators with a long barrier (FRLB) clearly show the formation of characteristic flow structures. In the case of series 2 and 3, a well-developed area of swirl motion was observed in the main part of the chamber, which indicates an effective flow stabilization. The presence of a stable vortex results in an effective dissipation of the liquid's kinetic energy, which in turn directly translates into lower values of the discharge coefficient (as can be seen in Table 4). In series 4, despite a less intensive swirl motion, a clear phenomenon of stream contraction occurs at the regulator's outlet, which leads to a local increase in flow losses. This mechanism also contributes to a reduction in the flow rate, but the values of the μ coefficient in this series are slightly higher than for the regulators from series 2 and 3. It is also worth noting that the design of the regulator affects the degree of filling of the swirl chamber and the uniformity of the flow field.

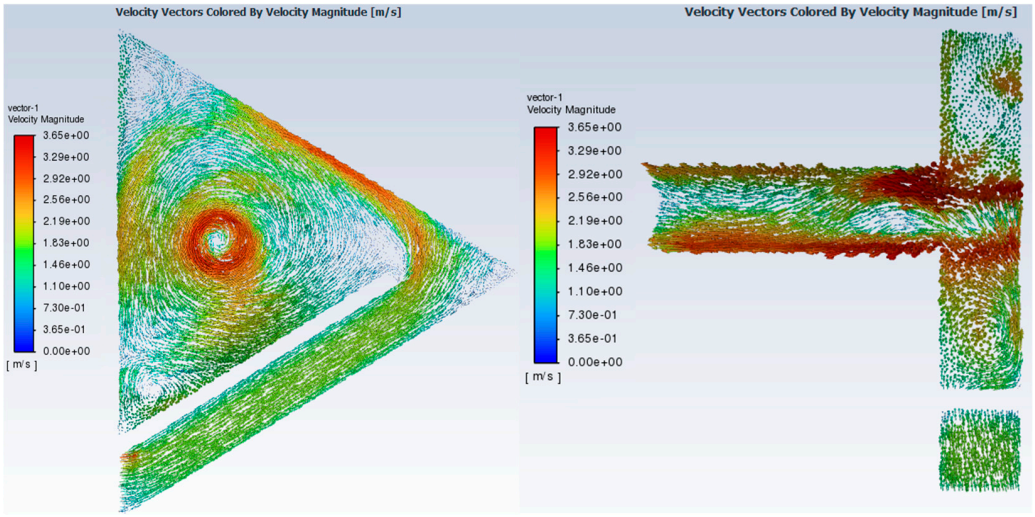

(**a**)

Figure 7. *Cont.*

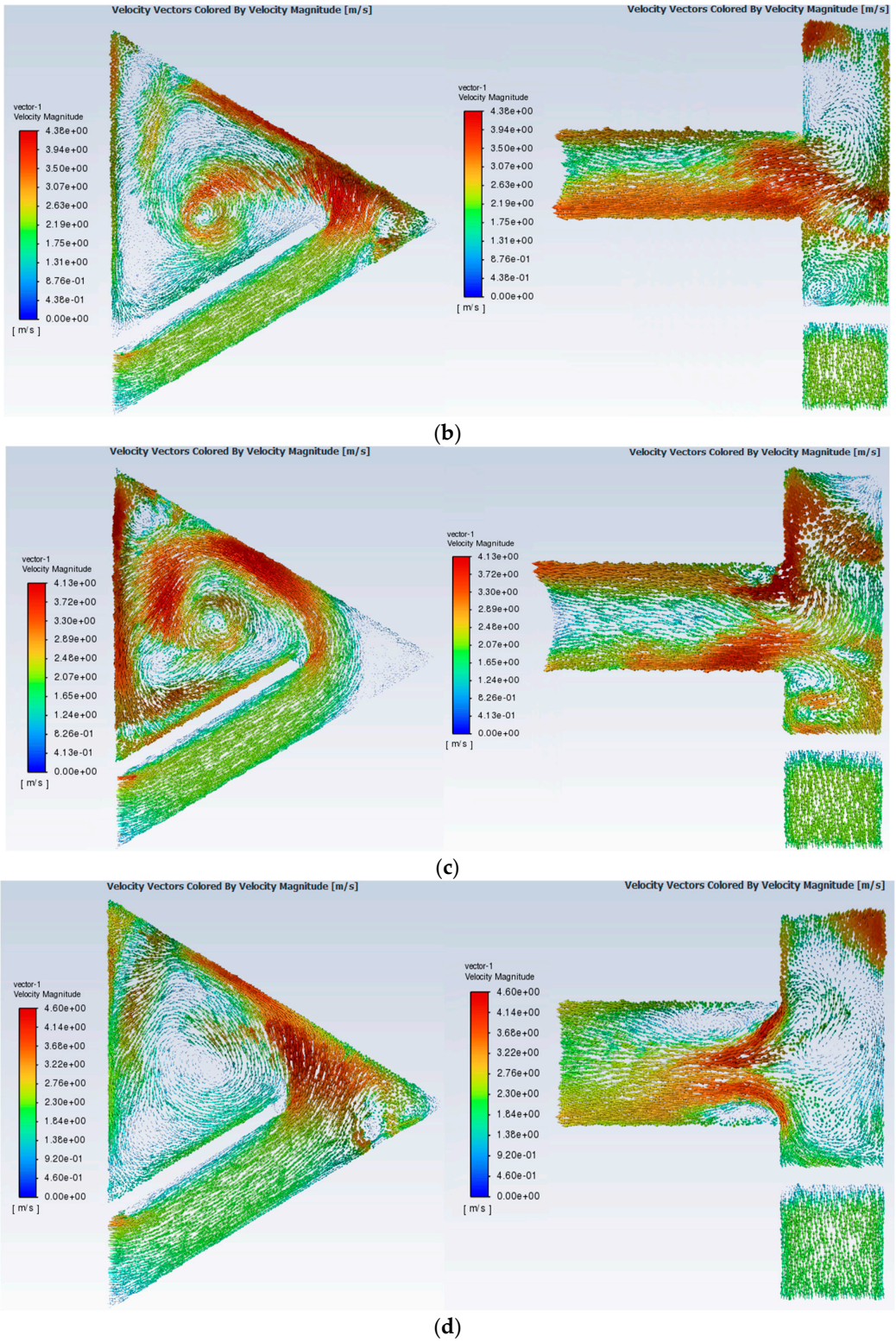

Figure 7. Field and velocity vector distributions for the regulators with a long barrier (FRLB): (**a**) series 1; (**b**) series 2; (**c**) series 3; (**d**) series 4.

4. Conclusions

The conducted experimental studies and CFD numerical analyses allowed for the formulation of several key observations concerning the influence of the design of flow regulators on their hydraulic characteristics. The obtained $Q(H)$ relations showed that the regulators equipped with a long barrier (FRLB) were characterized by the highest

efficiency of flow restriction, which was manifested by the low dynamics of the increase in the flow rate with regards to the height of the liquid column. The regulators with a short barrier (FRSB) had a moderate flow damping capacity, while the regulators without a barrier (FRWB) were characterized by a clearly higher flow sensitivity to an increase in the water damming level. This in turn indicated the limited effectiveness of the formation of the vortex flow. In this case, the flow rate increased almost proportionally to the liquid's height. The results of the analysis of the discharge coefficient with regards to the Reynolds number also confirmed these observations. The FRLB regulators achieved lower values of the discharge coefficient when compared to the FRSB and FRWB regulators. This was especially the case in series 2 and 3, which indicates a more effective flow restriction in systems with long barriers. The discharge coefficient values were stable in these cases with respect to changing flow conditions, which in turn indicates a high hydraulic stability of the structure. Analysis of the velocity field distributions and vectors obtained from the CFD simulations provided additional evidence for the effectiveness of the FRLB regulators. In variants of series 2 and 3, extensive stable areas of swirl motion were observed in the chamber. These were responsible for the higher kinetic energy losses and the effective limitation of the discharge intensity. In the case of series 4, despite the lower intensity of the swirl flow, the phenomenon of stream contraction was observed in the outlet area, which also contributed to the increased flow resistance and partial limitation of the liquid flow rate. Ultimately, the test results confirmed that the use of a long barrier in a triangular prismatic cross-section regulator significantly improves the ability to control the flow and also increases the stability of the device. The effectiveness of the FRLB variant results from the effective stabilization of the swirl motion in the chamber and the additional hydrodynamic effects, such as the stream contraction that was observed in the selected geometric configurations. The conducted CFD analysis requires further research, both in terms of the scope of modelling (including making the variability of boundary conditions more precise) and the completeness of input data. These activities are necessary for verifying the convergence of CFD simulation results with real experimental measurements. Full agreement between the numerical model and experimental results can be the basis for formulating reliable relationships between input data and the obtained effect.

Author Contributions: M.O. (Marek Ochowiak): conceptualization of the study, experimental design, data analysis, writing the original draft. D.J.: flow modeling, results analysis, critical revision of the manuscript. S.W.: preparation and execution of experiments, data collection. A.K.: support in result interpretation, preparation of data visualizations. M.M.: methodological consultation, manuscript review and editing. M.O. (Magdalena Olszewska): project supervision, approval of the final version of the manuscript. All authors have read and agreed to the published version of the manuscript.

Funding: This research was funded by the Ministry of Education and Science of Poland (SBAD).

Informed Consent Statement: Not applicable.

Data Availability Statement: The experimental and computational data generated during this study are available from the corresponding authors upon reasonable request.

Acknowledgments: The authors gratefully acknowledge the financial support provided by the Ministry of Education and Science of Poland (SBAD).

Conflicts of Interest: The authors declare no conflicts of interest.

References

1. Catano, Y.; Waratuke, A.R.; Garcia, M.H. Experimental investigation of a vortex-flow restrictor: Rain-blocker performance tests. *J. Hydraul. Eng.* **2010**, *136*, 8.
2. Ali, H.H.; Fales, R.C. A review of flow control methods. *Int. J. Dyn. Control.* **2021**, *9*, 1847–1854. [CrossRef]

3. Jarman, D.S.; Andoh, R.Y.G.; Tabor, G.; Butler, D. Modelling of vortex flow controls at high drainage flow rates. *Eng. Comput. Mech.* **2015**, *168*, 17–34. [CrossRef]
4. Faram, M.; Stephenson, A.G.; Andoh, R.Y.G. Vortex flow controls: State of the art review and application (from the catchbasin to the dam). In Proceedings of the Novatech: 7th International Conference on Sustainable Techniques and Strategies in Urban Water Management, Lyon, France, 28 June–1 July 2010.
5. Brombach, H. Flood protection by vortex valves. *Dyn. Syst. Meas. Control.* **1981**, *103*, 228–336. [CrossRef]
6. Smisson, R.P.M. The single pipe system for stormwater management. *Prog. Water Technol.* **1980**, *13*, 203–214.
7. Yin, J.; Jiao, L.; Wang, L. Large eddy simulation of unsteady flow in vortex diode. *Nucl. Eng. Des.* **2010**, *240*, 970–974. [CrossRef]
8. Pandare, A.; Ranade, V.V. Flow in vortex diodes. *Chem. Eng. Res. Des.* **2015**, *102*, 274–285. [CrossRef]
9. Qu, S.X.; Wu, Y.H.; He, Z.Z.; Chen, K. Surrogate fluid experimental study and CFD simulation on the hydraulic characteristics of vortex diode. *Nucl. Sci. Eng.* **2018**, *189*, 282–289. [CrossRef]
10. Parsian, H.; Butler, D. Laboratory investigation into the performance of an in-sewer vortex flow regulator. *Water Environ. J.* **1993**, *7*, 182–189. [CrossRef]
11. Siuta, T.; Mączałowski, A. Evaluation of vortex flow controls efficiency based on CFD numerical modelling. *Acta Sci. Pol. Form. Circumiectus* **2019**, *18*, 85–95. [CrossRef]
12. Kotowski, A.; Wójtowicz, P. Analysis of hydraulic parameters of cylindrical vortex regulators. *Environ. Prot. Eng.* **2008**, *34*, 43–56.
13. Wójtowicz, P.; Szlachta, M. Experimental investigation and prediction of oxygen transfer in vortex flow regulators. *Chem. Eng. J.* **2016**, *287*, 337–349. [CrossRef]
14. Zhu, Y.; Lu, Y.; Wu, Y.; Zhang, J.; Chen, G.; Zhang, G.; Wu, Z. Numerical investigation of fine sand removal in vortex-enhanced spiral pipeline separators via coupled CFD-DEM simulation. *Powder Technol.* **2026**, *469*, 121702. [CrossRef]
15. Weng, Z.; Qian, Y.; Zhu, D.Z.; Mugume, S.N. Evaluation on the performance of a swirling-type hydrodynamic separator using physical and numerical models. *Water Sci. Technol.* **2024**, *90*, 344–362. [CrossRef] [PubMed]
16. Mahaveer; Zima, P.; Qaisrani, M.A.; Kalwar, M.A. Review of current approaches and gaps in modeling hydrodynamic vortex separator for enhanced separation efficiency. *Desalination Water Treat.* **2025**, *324*, 101426. [CrossRef]
17. He, W.; Chen, Y.; Zhang, P.; Zhang, Q.; Ma, J. CFD-based prediction of vortex-induced turbulent flow in urban stormwater manholes: Insights into gravity and pressure flow dynamics. *J. Water Process Eng.* **2025**, *77*, 108346. [CrossRef]
18. Armtec. Hydro-Brake® Flow Control. Available online: https://armtec.com/products/hydro-brake-vortex-flow-control (accessed on 22 April 2025).
19. Wavin. Vortex Flow Regulators: Tornado, Typhoon, Hurricane. Available online: https://wavin.com/ie/s/C02_F005_S014/Vortex-Flow-Control-Valves (accessed on 22 April 2025).
20. Oksydan Sp. z o.o. Regulatory Wirowe. Available online: https://oksydan.pl/kategorie-produktow/regulatory-przeplywu (accessed on 22 April 2025).
21. Andel. Vortex Flow Control. Available online: https://www.andel.com/products/vortex-flow-control (accessed on 22 April 2025).
22. Karbowska, P.; Kamola, I. Design and Testing of Vortex Flow Regulators. Master's Thesis, Poznan University of Technology, Poznan, Poland, 2019.
23. Ecol-Unicon. Available online: https://ecol-unicon.com/systemy-kontroli-przeplywu/regulatory-przeplywu (accessed on 14 November 2024).
24. Olszewska, M. Tests of Hydrodynamic Regulators with Swirling Elements. Master's Thesis, Poznan University of Technology, Poznan, Poland, 2025.
25. Stora, s.r.o. Available online: https://stora.cz/en/products/flowregulators/whirlregulatorsvortex/regulatorvortexcye (accessed on 1 October 2025).
26. KM Instal Sp. z o.o. Available online: https://kminstal.pl/regulatory/ (accessed on 1 October 2025).
27. Hydros, S.C. Available online: https://www.facebook.com/hydros.separatory (accessed on 1 October 2025).
28. Olszewska, M.; Włodarczak, S.; Krupińska, A.; Ochowiak, O.; Ochowiak, M. The study of triangular flow regulators. In Proceedings of the 12th International Conference on Sustainable Solid Waste Management, Paphos, Cyprus, 25–28 June 2025.
29. Olszewska, M.; Ochowiak, M. The study of triangular flow regulators. In Proceedings of the 1st International Conference PUT STEM Day 2025: Book of Abstracts, Poznan, Poland, 10 January 2025.
30. Susdrain. Available online: https://www.susdrain.org/delivering-suds/using-suds/suds-components/inlets-outlets-and-control-structures/vortex-control-systems (accessed on 1 October 2025).
31. Freeflush Water Management. Available online: https://www.freeflush.co.uk/products/stainless-steel-vortex-flow-control-device (accessed on 1 October 2025).
32. Scotia Supplies. Available online: https://www.scotia-supplies.com/product/vortex-flow-control/ (accessed on 1 October 2025).

33. Kopiński, M.; Ochowiak, M.; Włodarczak, S.; Krupińska, A. Modeling box-type flow control systems and comparing them with standard design solutions. In Proceedings of the 4th Practical Seminar on Aspects of Chemical Engineering, Zaniemyśl, Poland, 16–17 May 2024.
34. Hydro International. Available online: https://www.hydro-international.com/hydrographic-industry-showcase (accessed on 17 November 2024).
35. Kopiński, M. Modeling Box-Type Flow Control Systems and Comparing Them with Standard Design Solutions. Bachelor's Thesis, Poznan University of Technology, Poznan, Poland, 2025.
36. ANSYS, Inc. *Ansys Fluent Theory Guide, Release 2023 R2*; ANSYS, Inc.: Canonsburg, PA, USA, 2023.

Disclaimer/Publisher's Note: The statements, opinions and data contained in all publications are solely those of the individual author(s) and contributor(s) and not of MDPI and/or the editor(s). MDPI and/or the editor(s) disclaim responsibility for any injury to people or property resulting from any ideas, methods, instructions or products referred to in the content.